Performance Improvement of LC-Based Beam-Steering Leaky-Wave Holographic Antenna Using Decoupling Structure

Hyungcheol Kim and Sangwook Nam, *Senior Member, IEEE*

***Abstract*—A liquid crystal-based beam-steering leaky-wave holographic antenna is designed with decoupling structure. Since the distance between elements in holographic antennas is inevitably small (<λ/5), the mutual coupling is strong and should be compensated for the accurate implementation of the excitation amplitude and phase of each element. The performance degradation of a holographic antenna due to mutual coupling is estimated and a decoupling structure is proposed, fabricated, and inserted into the designed antenna. The operating principle of the decoupling structure is explained with circuit model and the simulation confirms the enhanced gain and sidelobe performance when steered from −60° to 60° in 20° intervals. Compared to the antenna without the decoupling structure, the maximum improvement of the gain and the sidelobe level is 3.93 and 7.7 dB, respectively, in the simulation. The experimental results are consistent with the simulation results.**

***Index Terms*—Beam scanning, beam steering, decoupling, holographic antenna, holographic method, leaky wave, liquid crystal (LC).**

I. Introduction

BEAM-STEERING antennas are traditionally designed using a phased array. However, it is expensive and bulky system with a high loss in the feed network and phase shifters at high frequencies [1], [2]. Therefore, various beam-steering methods without phase shifters have recently attracted much attention [3]–[16]. One of them is the leaky-wave antenna that uses reconfigurable components, such as varactor, p-i-n diodes, or liquid crystal (LC) [6]–[16]. The leaky-wave antenna has the advantages of high directivity, low cost, and low profile. Its basic radiation properties and design methodologies have been extensively studied [17]–[22]. Especially, Smith *et al.* [22] described several element modulation methods using a holographic method.

Generally, an antenna designed using resonance-based holographic method has a small distance between the cells involved in radiation, resulting in coupling between the cells [12]–[16], [22], [23]. The discrete dipole approximation model that includes the coupling effects has been used with an optimization technique to design holographic antennas [16]. It would be ideal to design a holographic antenna taking such couplings into consideration. However, such a design is difficult as the cell states vary dynamically with the steering angle. Therefore, in many cases, holographic beam-steering antennas have been designed based on the characteristics extracted from the unit cell under the assumption that the cell operates independently without coupling [12], [13], [22]. However, neglecting the coupling degrades the actual performance of the antenna in terms of gain and sidelobe level (SLL), compared to the expected performance.

There are two representative methods to reduce the mutual coupling. The first one is to increase the distance between the elements. However, such a method can generate critical grating lobe, and the beam-steering range can reduce significantly. Recently, the coupling was reduced by placing cells alternately at both edges of the substrate integrated waveguide (SIW) to widen the effective distance [14]. Another simple method is to reduce the radiation intensity of each cell by reducing the perturbation to the guided wave [10]–[13]. However, such a method may reduce the efficiency and gain due to large feeding loss.

In this study, a decoupling structure that reduces the coupling between the cells was proposed. The designed decoupling structure can be used to reduce the gap between the expected and real performances. To demonstrate this, an LC-based holographic antenna with decoupling structure was designed, which could configure the main beam direction from −60° to 60° at 10 GHz. The simulation results demonstrated improved performance than the design without the decoupling structure. The antenna, including the decoupling structure, was fabricated and tested.

The contents of this article are as follows. Section II discusses the basic principle of holographic antenna and the design of beam-steering antenna. In Section III, we design an antenna that satisfies all the conditions mentioned in Section II. The coupling between two elements and performance degradation due to the coupling is identified. In Section IV, a decoupling structure is proposed. The complete holographic antenna with the proposed structure is simulated. The operation of the proposed decoupling structure is explained with the circuit model. In Section V, the fabricated antenna and test setup are shown, and the measurement results are presented.

Manuscript received May 28, 2021; revised August 30, 2021; accepted September 22, 2021. Date of publication October 14, 2021; date of current version April 7, 2022. This work was supported by the Institute of Information and Communications Technology Planning and Evaluation (IITP) grant funded by the Korea Government (MSIT) (Development of key technologies for 6G Radio Frequency (RF) front-end based on low-power multiple-input and multiple-output (MIMO) and highly efficient spatial Quadrature Amplitude Modulation (QAM) synthesis) under Grant 2021-0-00198. *(Corresponding author: Sangwook Nam.)*

The authors are with the School of Electrical and Computer Engineering, Institute of New Media Communication, Seoul National University, Seoul 152742, South Korea (e-mail: hckim8@ael.snu.ac.kr; snam@snu.ac.kr).

Color versions of one or more figures in this article are available at https://doi.org/10.1109/TAP.2021.3118779.

Digital Object Identifier 10.1109/TAP.2021.3118779

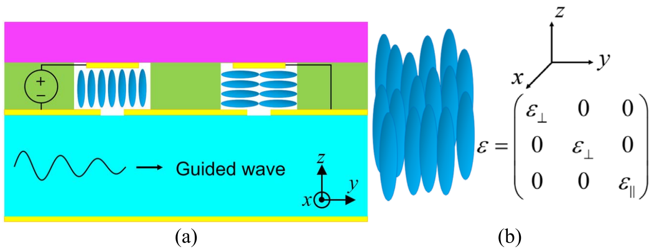

Fig. 1. (a) Longitudinal cross-sectional structure of the designed holographic antenna controlled with LC. (b) Shape of LC molecule and its permittivity tensor.

II. Holographic Antenna Principle, Realization, and Design Consideration

In holographic antennas, the reference wave excites the radiating elements at different positions on the interference plane as it passes through a guiding structure. The summation of the field radiated by all radiating elements generates the desired wave. The basic formula of the holographic method is as follows [16]:

$$\Psi_{des} = \Psi_{int}\Psi_{ref} \tag{1}$$

where Ψ_{des} and Ψ_{ref} are the desired far-field wave and reference wave that illuminate recorded pattern on a plane, respectively. Interference wave Ψ_{int} is recorded on the plane. It is the polarizability at each position in the plane required to generate the desired radiation when excited by the reference wave. Once the desired and reference waves are determined, the type of modulation that should be implemented on the interference plane can be determined.

The reference wave used in this study is the TE10 mode of the SIW, and the y-direction is the propagating direction of the guided wave. The desired wave corresponds to the beam pattern with the main beam in the desired direction. The modulation on the plane is realized by a slot-coupled patch cell, where a patch is excited by a slot etched on the SIW surface, and an LC is filled in the cavity box formed between the slot and the patch. The LC box acts as a substrate for the slot-coupled patch cell, as shown in Fig. 1(a). It can be used to control the resonant frequency of slot-coupled patch cell by applying a specific voltage to the patch and adjusting the molecule alignment as used in the LC display technology. Fig. 1(a) shows the overview and the molecular alignment state depending on whether the voltage is applied. When voltage is applied to an LC molecule, it is forced to align in a specific direction. If no voltage is applied, the LC molecule is aligned parallel to the surface because there is no electric field that exerts an alignment force on the molecule. Because LCs are anisotropic materials as shown in Fig. 1(b) [24], the effective dielectric constant of each cell varies depending on the alignment of the LC. Therefore, the radiation characteristics of the single cell also change, which allows configurable modulation for each radiating element.

The methodology discussed above was applied to design an antenna capable of steering from $-60°$ to $60°$ at 10 GHz. The appropriate amplitude modulation for generating the main beam in the desired direction is as follows [22]:

$$\Psi_{int} = \frac{\cos((\beta - k\sin\theta)y) + 1}{2}, \quad \Psi_{ref} = e^{-j\beta y} \tag{2}$$

$$\Psi_{des} = \frac{e^{-jk\sin\theta y}}{4} + \frac{e^{-j(2\beta - k\sin\theta)y}}{4} + \frac{e^{-j\beta y}}{2} \tag{3}$$

where β is the wavenumber of the reference wave, k is the free space wavenumber, and θ is the main beam angle. The cosine function is used as the base form and a constant is added to make the amplitude positive. Applying Fourier analysis to (3) confirm the occurrence of three terms. The first term is the ideal modulation, which generates the main beam in the desired direction, and the second and the third are modulation terms that can possibly generate beams in undesired directions, which may act as grating lobes. The main conditions to be considered for prevention of grating lobes are as follows [22]:

$$2\beta - k\sin\theta > k \quad \text{for} \ -60° \le \theta \le 60° \tag{4}$$

$$\beta > k. \tag{5}$$

If condition (5) is satisfied, (4) is satisfied as well. In addition to the above two conditions, further conditions are needed as the modulation of the corresponding holographic antenna is not continuous. The basic structure to be designed is a slot-coupled patch cell excited by the TE10 mode, and it is reasonable to consider each cell as a discrete radiating element rather than a spatially continuous one. The spacing between cells, that is, the spacing at which the modulation is actually achieved, is denoted as d, and the spatial sampling frequency is denoted as $P_s (= 1/d)$. The additional conditions to prevent grating lobes because of spatial sampling are as follows:

$$k < 2\beta - k\sin\theta + 2\pi m P_s \ \ or \ \ 2\beta - k\sin\theta + 2\pi m P_s < -k \tag{6a}$$

$$k < \beta + 2\pi m P_s \ \ or \ \ \beta + 2\pi m P_s < -k \tag{6b}$$

$$k < k\sin\theta + 2\pi m P_s \ \ or \ \ k\sin\theta + 2\pi m P_s < -k \tag{6c}$$

$$for\ every\ m = \pm 1, \ \pm 2, \ \pm 3 \ldots$$

To avoid grating lobes, the post-sampling Fourier spectrum must not have any components in the visible region. The sufficient conditions are organized in (6). If (6a) is satisfied for $\theta = -60°$, (6b) and (6c) conditions are found to be satisfied as well for $-60° \le \theta \le 60°$.

The implementation of the cosine modulation is difficult as each cell controlled by an LC is modulated not only in amplitude but also in phase due to the varying alignment of the LC. Accordingly, the cosine modulation was mapped to 0 and 1 only. The mapping equation is as follows [22]:

$$\begin{aligned}\Psi_{int}(y) &= 0 \ if \ \ \cos((\beta - k\sin\theta)y) \le 0 \\ &= 1 \ if \ \ \cos((\beta - k\sin\theta)y) > 0. \end{aligned} \tag{7}$$

After mapping the cosine modulation into a one-bit scheme, it should also be verified that such a mapping procedure does not generate any critical grating lobes. This will be confirmed in Section III, where the propagation constant of the guided wave β and the spacing between the radiating elements d are determined by designing the single-cell model.

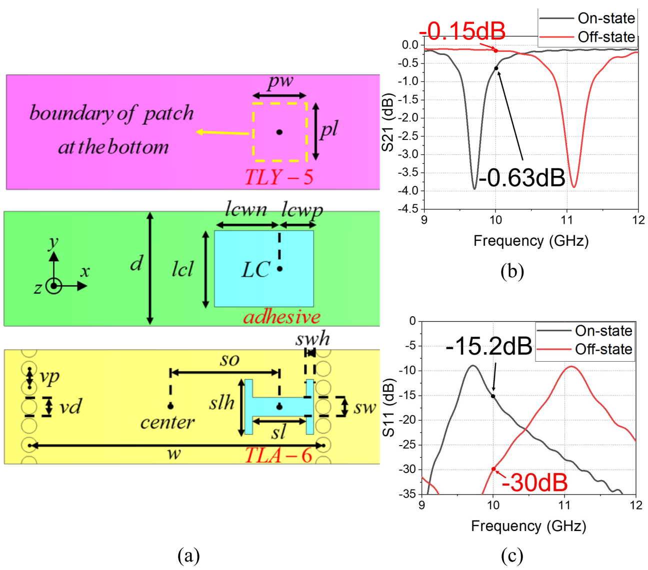

Fig. 2. Single-cell design. (a) Top view of simulated model of each layer. The characteristics of (b) S_{21} and (c) S_{11} changes depending on the control of LC.

TABLE I
DIMENSIONS FOR ANTENNA (UNIT: mm)

t	vd	vp	d	sw	swh	sl		slh*		pl*	
0.035	0.8	1	6	1	0.4	2.8		2.9	2.8	3	2.8
pw	so	lcl	lcwp	lcwn	w	rl*		rw*		rg*	
2.8	5.4	4	1.8	3.4	15.4	N/A	5.4	N/A	0.1	N/A	0.1

t: thickness of copper. *Left: without decoupling. *Right: with decoupling.

III. SINGLE-CELL DESIGN WITHOUT A DECOUPLING STRUCTURE

A. Single-Cell Structure

The basic structure of the single element was the slot-coupled patch excited by the TE10 mode guided by SIW, and the operating frequency was set to 10 GHz. Fig. 2(a) shows the top view of single-cell model of the three layers. All specific dimensions are listed in Table I.

The bottom layer of the complete antenna was constructed using TLA-6 from Taconic Corporation. The dielectric constant and loss tangent were 2.62 and 0.002, respectively. The thickness of the substrate was 1.96 mm. The bottom layer was SIW, and a slot was etched on the top surface to allow coupling with the radiating elements. The slot was etched near the edge of the SIW to reduce perturbation to the original reference wave. The slot was H-shaped to reduce the resonant frequency of the slot-coupled patch within limited footprint.

The second layer was an adhesive layer that acts as a spacer to trap LCs. It connects the upper and lower substrates while leaving space for the LC to be filled. The height was set to 300 μm. The LC used in this antenna was GT7-29001 (Merck). The $\varepsilon_{||}$ and $\varepsilon_{\perp}$ values of the LC were 3.5338 and 2.4562, respectively. In addition, the loss tangent for the corresponding directions was 0.0064 and 0.0116, respectively.

The third layer acts as a lid to completely trap the LC, which can leak otherwise. The substrate is TLY-5 from Taconic Corporation. The dielectric constant and loss tangent are 2.2 and 0.0009, respectively. The thickness of the substrate was 0.25 mm. There exists a patch on the lower surface of the substrate that acts as a radiating structure in pairs with the slot in the first layer. In addition, a voltage was applied to this patch to control the LC alignment.

TABLE II
MODULATION STATE OF 43 ELEMENTS FOR EACH BEAM STEERING

Targeted beam position	Modulation state
-60°	1010010101101010110101001010100101011010101
-40°	1011010010110100101101001011010010100101101
-20°	1001001101101101100100100100110110110110010
0°	1001100110011001100110011001100110011001100
20°	1100011000111000110001110001100011100011000
40°	1110000111100001111000011110000111100000111
60°	1111000000111111100000011111110000000111111

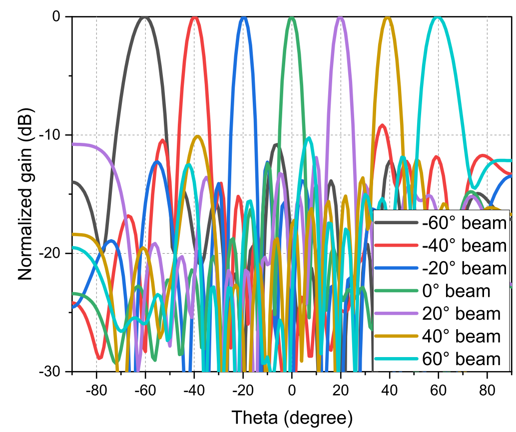

Fig. 3. Calculated array factor of the holographic antenna using 1 bit modulation scheme in Table II.

B. Beam-Steering Capability With Ideal Condition

With β (262 rad/m $= 1.251k$) extracted from the model of SIW without any modulation by using CST studio suite 2021, the designed single model can be said to satisfy (5) and (6) in Section II. In addition, as we use the one-bit scheme in cosine modulation, it should be confirmed that the scheme does not generate any critical sidelobe. Therefore, the array factor produced by applying (7) was calculated for 43 elements while assuming small perturbation to the original reference wave and minor energy leakage. The modulation of the one-bit scheme for the designed model is specified in Table II. Fig. 3 shows the normalized array factor results when the beam is steered from $-60°$ to $60°$ with $20°$ intervals. The results show that the real main beam position is formed near the targeted direction and the worst case scenario for SLL is 9.2 dB, indicating that the simple one-bit modulation scheme is acceptable for this design.

C. Single-Cell Characteristics

To examine the resonant characteristics of the corresponding unit cell, the TE10 mode is excited into the SIW structure,

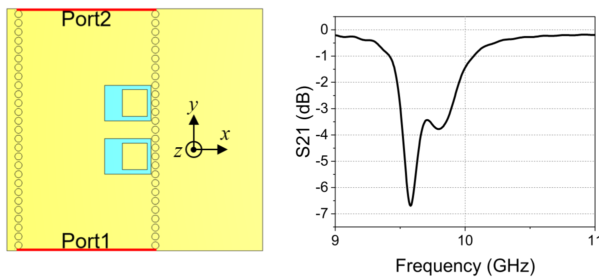

(a) (b)

Fig. 4. Coupling effect between two elements in holographic antenna. (a) Two cells without decoupling structure. (b) S_{21} of (a).

and the S-parameter is examined. The LC is modeled as an isotropic material for convenience. The tensor element in the z-direction is used in the isotropic model to determine the resonant frequency for each bias state. Fig. 2 (b) and (c) shows the S_{11} and S_{21} results, respectively, with and without the full bias. As shown, the resonant frequency decreases with the increase in the dielectric constant, and the resonant frequency shifts from 9.7 to 11 GHz. The OFF-state is used as mapping 0 in (7), as its high S_{21} level means little radiation at 10 GHz in this state. It would be preferable to realize mapping 1 with the exact resonant frequency at 10 GHz; however, this can cause large amounts of reflection and rapid attenuation of the guided wave, which is inconsistent with the assumption of holographic antenna design. Therefore, the ON-state, which has a resonant frequency slightly shifted from 10 GHz, is used for mapping 1 in (7), implying that a reasonable amount of power is radiated through the single element as the TE10 mode passes.

D. Coupling Effect

The simulation model used to confirm the coupling effect between the two elements is shown in Fig. 4(a). Two cells in the ON-state are attached with spacing d. Fig. 4(b) shows the S_{21} results of the model. In Fig. 4(b), the resonance frequency is split due to the coupling between the two resonators with the same resonant frequency. In addition, the difference in the phase of the current flow in each patch is found to be $-47.2°$. If there is no coupling between them, the phase difference should be $-\beta d\,(\approx -90.1°)$ according to the assumption of holographic antenna design; however, the extracted phase difference is different from the expected value. This suggests that the presence of coupling between cells will prevent the holographic antenna from working properly, as expected.

E. Complete Design Result

The complete design of the holographic antenna consisting of 43 elements, which is applied with the same one-bit modulation scheme in Table II, was simulated. Beam-steering performance was tested for seven patterns steering from $-60°$ to $60°$ with $20°$ intervals. The obtained beam patterns are shown in Fig. 5. The results clearly show the deterioration caused by the coupling between the elements. Notice the SLL is poor when the beam is steered from $20°$ to $60°$ since the ON-states appear in a row frequently in this modulation range:

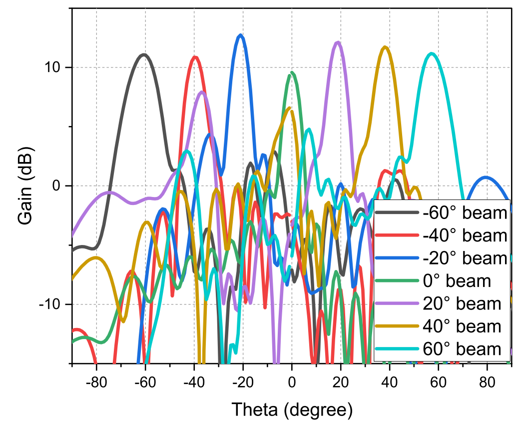

Fig. 5. Simulated gain of 43 elements holographic antenna without decoupling structure.

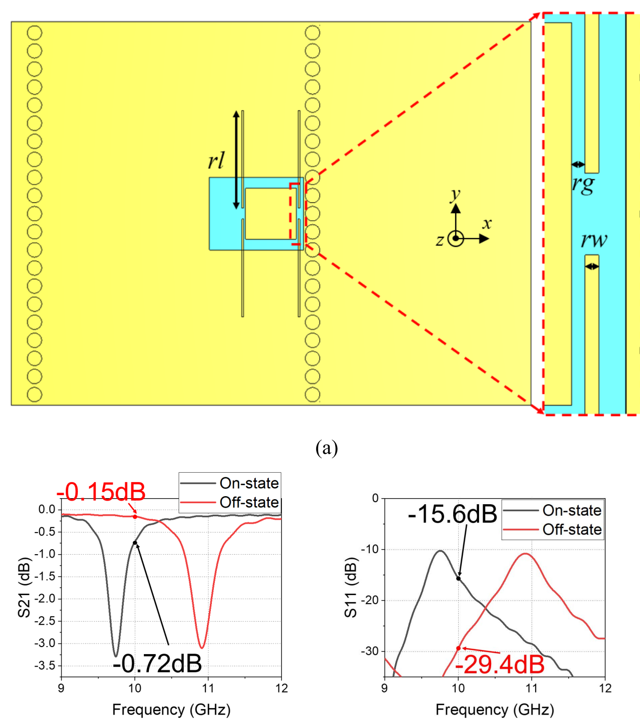

(a)

(b) (c)

Fig. 6. (a) Single-cell model with decoupling structure. The dependence of (b) S_{21} and (c) S_{11} on the control of LC.

the ON-state resonators having the same resonant frequency are coupled with each other and break the proper phase relations between the elements.

IV. Single-Cell Design With Decoupling Structure

A. Single-Cell Structure and Characteristics

The unit cell with decoupling structure was redesigned and shown in Fig. 6(a). Thin strip lines were added to the same layer of the patch. Dimensions of the decoupling structure are optimized and some original dimensions are slightly adjusted to achieve the resonant frequency of the previous model. These are shown in Table I. Fig. 6(b) and (c) shows S_{21} and S_{11} of the redesigned single cell, respectively, with and without full bias voltage.

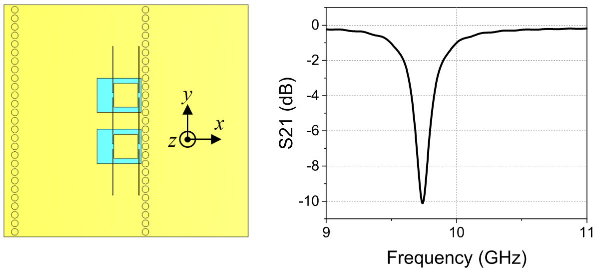

Fig. 7. (a) Simulation model of two cells with decoupling structure. (b) S_{21} of (a).

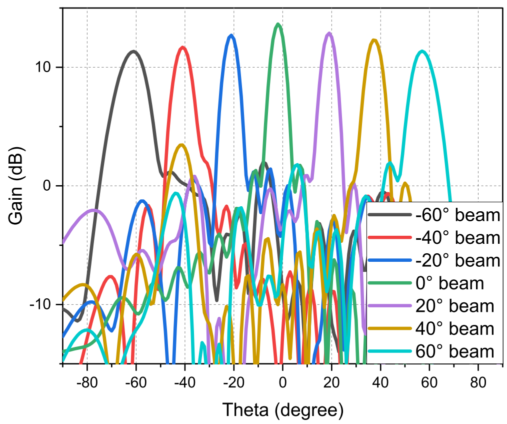

Fig. 8. Simulated gain of 43 elements holographic antenna with decoupling structure.

B. Decoupling Test

Finally, we checked the S_{21} parameters for the two cells and the phase of the current applied to each patch to verify that the unit cell was properly decoupled. The two-cell simulation model with the decoupling structure is shown in Fig. 7(a). It was excited by the TE10 mode, and the S_{21} result in Fig. 7(b) shows that the resonant frequency is not split. The phase of the current flow in each patch was checked and the phase difference was confirmed to be $-98.5°$, which is close to the designed value $-\beta d$ ($\approx -90.1°$) compared with $-47.2°$ without a decoupling structure shown in Section III-C. These results indicate that the designed decoupling structure works properly.

C. Complete Design Result

As in the previous design, a total of 43 elements were constructed, and a total of seven patterns were identified by steering between $-60°$ and $60°$ with $20°$ intervals. The mapping scheme shown in Table II was reapplied. The results are presented in Fig. 8. The improvement in the gain and SLL relative to the antenna without the decoupling structure is shown in Fig. 9. Through the simulation, the 3 dB gain bandwidth was found to be 200, 190, 210, 190, 240, 240, and 270 MHz at $-60°$, $-40°$, $-20°$, $0°$, $20°$, $40°$, and $60°$ steering angles, respectively.

D. Circuit Model and Mechanism of Coupling and Decoupling

The designed radiating element can be represented as an approximate circuit model. The coupling and decoupling mechanism can be explained by inductive coupling between two adjacent parallel resonators. For every circuit simulation in this study, ADS 2021 was utilized.

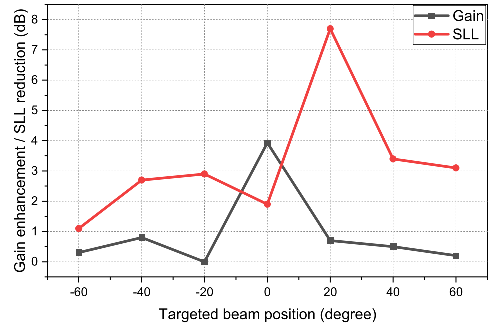

Fig. 9. Gain enhancement and SLL reduction of the holographic antenna with decoupling structure compared with the antenna without the decoupling structure.

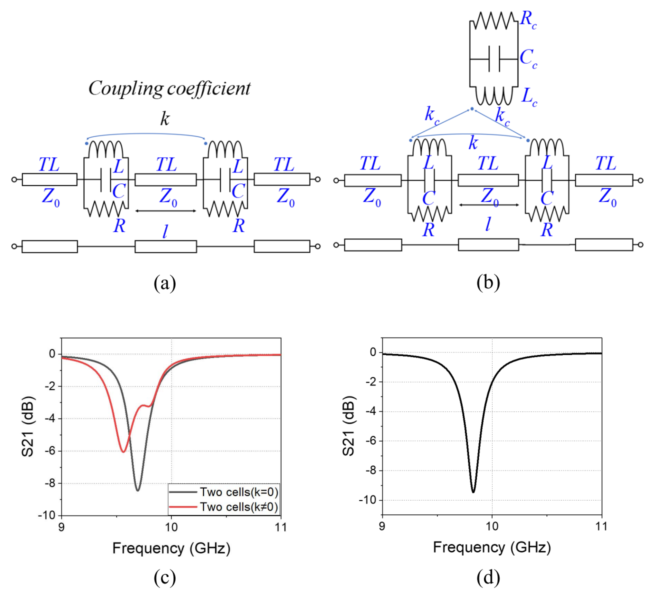

Fig. 10. Equivalent circuit model and the simulation results. (a) Two cells circuit model without the decoupling structure. (b) Two cells circuit model with the decoupling structure. (c) S_{21} of (a). (d) S_{21} of (b).

The two-cell simulation conducted by CST without the decoupling structure is approximately reproduced using the circuit model shown in Fig. 10(a). The S_{21} results of the circuit simulation with and without inductive coupling are shown in Fig. 10(c) where the resonant frequency splitting similar to the results shown in Fig. 4(b) appears with inductive coupling. The phase difference between two resonators deviates from the desired value ($-\beta d$) by 44.8°.

Fig. 10(b) shows the circuit model, including the decoupling resonator. The parallel resonator is designed to have a low R_c and resonates at approximately 16 GHz, which is higher than the operation frequency. The S_{21} result is shown in Fig. 10(d). There is no split in the resonant frequency, and this result is similar to that of S_{21} for $k = 0$ as shown in Fig. 10(c), corresponding to no inductive coupling between the two adjacent resonators. Also, it is consistent with the result of two-cell field simulation with the decoupling structure, as shown in Fig. 7. Notice that the deviation of the phase difference between two

TABLE III
CIRCUIT PARAMETERS FOR THE PROPOSED EQUIVALENT CIRCUIT

R	L	C	l	k	kc	Lc	Cc	Rc	Z_0
58Ω	0.0162nH	16.67pF	3.8mm	0.036	0.17	1nH	0.1pF	1Ω	50 Ω

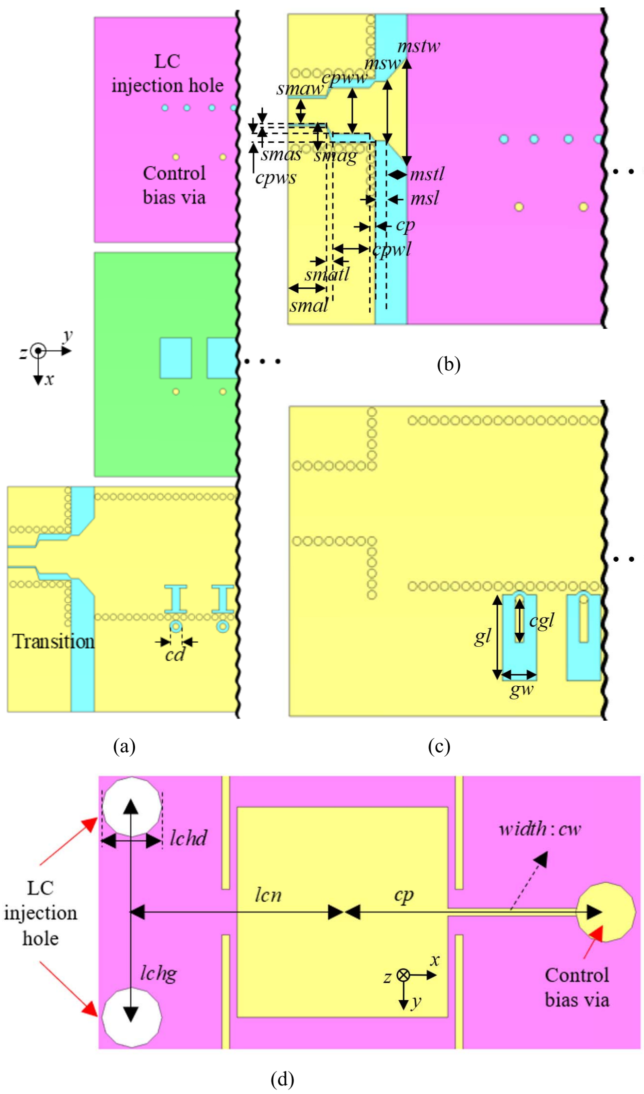

Fig. 11. Final antenna profile showing the first two elements of the designed antenna. (a) Top view of each layer shows the input transition, the control via, and LC injection holes. (b) Top view of the assembled structure and its dimensions. (c) Bottom view of the designed antenna. Area near the control via is etched out for connection with bias lines. (d) Bottom view of TLY-5 showing a patch, decoupling structure, bias line, and LC injection holes.

resonators is reduced to 5.4°, which is much smaller than 44.8° observed without the decoupling structure.

To summarize, inserting a new resonator to create extra inductive coupling cancels out the existing coupling. Table III lists all the values of the circuit components used in the circuit simulation.

V. FABRICATED ANTENNA AND MEASUREMENT

The fabricated antenna and the final profile are shown in Fig. 11. It consists of three layers and is stacked using a commonly used PCB process. Bias circuit with RF choke structure was added to apply voltage to each patch. This addition did not significantly affect the radiation characteristics described in Section IV. The specific dimensions of all three layers are listed in Table IV.

TABLE IV
DIMENSIONS FOR INCIDENTAL STRUCTURE (UNIT: mm)

cd	cgl	gl	gw	lchd	lchg	lcn	cp	cw	mstw	mstl
1.6	4	8	3.2	0.8	2.8	2.8	3.5	0.1	10	2
msw	msl	cpwtl	cpww	cpws	cpwl	smatl	smaw	smas	smag	smal
5.5	1	0.5	4.3	0.8	3.55	0.5	2.4	0.2	2.1	3.55

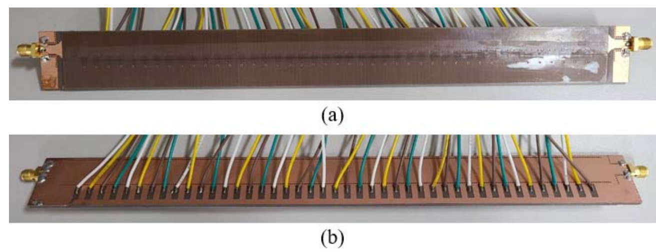

Fig. 12. Fabricated antenna. (a) Top view of the antenna. (b) Bottom view of the antenna.

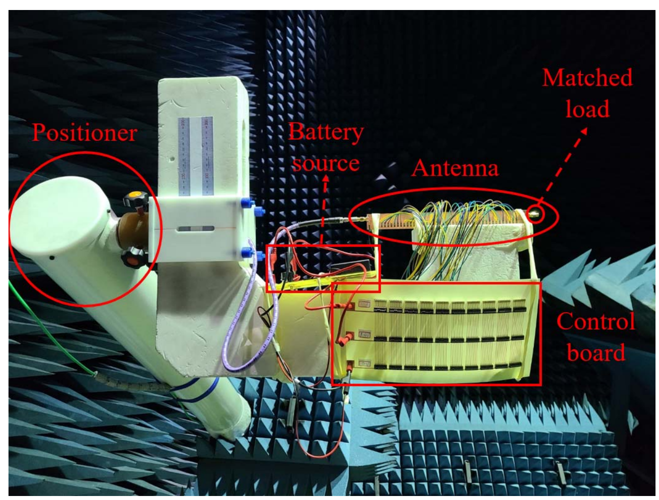

Fig. 13. Experimental setup for measurement of the fabricated antenna pattern.

The manufactured antenna is shown in Fig. 12. On the lower side of the antenna, the via connected to each patch is soldered separately to connect to the control board. Finally, a voltage of 32 V was applied to realize the ON-state, and ground potential was applied to realize the OFF-state. The appropriate operating frequency is identified as 10.1 GHz due to slightly shifted resonant frequency. Therefore, the beam pattern was measured at 10.1 GHz using the measurement setup shown in Fig. 13. The modulation scheme was applied, as shown in Table II.

The measurement results of the radiation pattern are shown in Fig. 14. The actual steering angle deviated slightly from the targeted steering angle. This is because the fabricated antenna

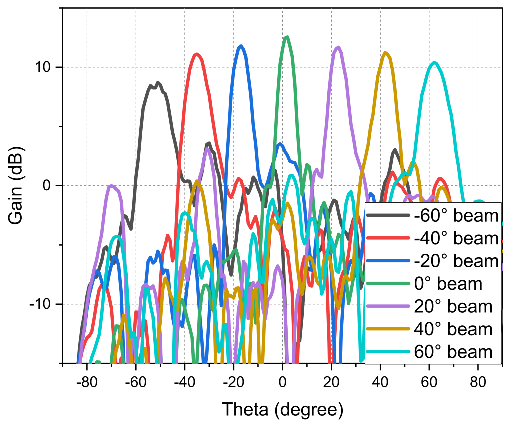

Fig. 14. Measured gain of the designed holographic antenna with decoupling structure for each beam steering.

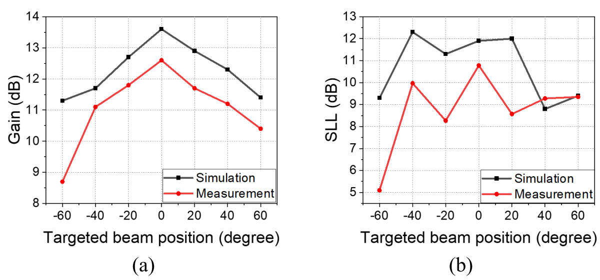

Fig. 15. Comparison between simulation and measurement. (a) Gain. (b) SLL.

operates at 10.1 GHz, while the applied modulation scheme is targeted at 10 GHz. This is consistent with the characteristics of the basic leaky-wave antenna. The comparison of measured gain and SLL with the simulation is shown in Fig. 15. The measured results agree with the simulation reasonably well. The inferior performance at the steering of −60° is due to the positioner in the measurement setup at that angle. In addition, the fabrication error, oblique alignment of LC by the floating dc voltage of the decoupling structure, and the assumption of isotropy for LC in the simulation may be the causes of difference between the simulation and the measurement.

VI. Conclusion

In this study, a leaky-wave resonance-based holographic antenna is designed, which can scan for different directions at 10 GHz with digital control on LC. Performance degradation by coupling between two adjacent elements is demonstrated and, to counter that, a decoupling structure is devised with explanation of the coupling reduction mechanism in terms of a circuit model. The enhanced antenna performance using the proposed decoupling structure was confirmed by computer simulation. The measured experimental results were consistent with the simulation results.

The proposed decoupling method adds an extra coupling path to cancel the original coupling between resonators. Besides holographic antenna, this methodology can be implemented for any general application using coupled resonant elements in close arrangement where the reduction of coupling between elements is desired. For a reconfigurable arrangement, the method and degree of coupling vary with variations in the state, degrading the overall performance of the arrangement. The decoupling mechanism proposed here can prevent such degradation by allowing each element to operate independently.

References

[1] C. Ding, Y. J. Guo, P.-Y. Qin, and Y. Yang, "A compact microstrip phase shifter employing reconfigurable defected microstrip structure (RDMS) for phased array antennas," *IEEE Trans. Antennas Propag.*, vol. 63, no. 5, pp. 1985–1996, May 2015.

[2] X. Ding, B.-Z. Wang, and G.-Q. He, "Research on a millimeter-wave phased array with wide-angle scanning performance," *IEEE Trans. Antennas Propag.*, vol. 61, no. 10, pp. 5319–5324, Oct. 2013.

[3] A. A. Baba, R. M. Hashmi, K. P. Esselle, M. Attygalle, and D. Borg, "A millimeter-wave antenna system for wideband 2-D beam steering," *IEEE Trans. Antennas Propag.*, vol. 68, no. 5, pp. 3453–3464, May 2020.

[4] P. Mei, S. Zhang, and G. F. Pedersen, "A low-cost, high-efficiency and full-metal reflectarray antenna with mechanically 2-D beam-steerable capabilities for 5G applications," *IEEE Trans. Antennas Propag.*, vol. 68, no. 10, pp. 6997–7006, Oct. 2020.

[5] R. Reese *et al.*, "A millimeter-wave beam-steering lens antenna with reconfigurable aperture using liquid crystal," *IEEE Trans. Antennas Propag.*, vol. 67, no. 8, pp. 5313–5324, Aug. 2019.

[6] M. Wang, H. F. Ma, H. C. Zhang, W. X. Tang, X. R. Zhang, and T. J. Cui, "Frequency-fixed beam-scanning leaky-wave antenna using electronically controllable corrugated microstrip line," *IEEE Trans. Antennas Propag.*, vol. 66, no. 9, pp. 4449–4457, Sep. 2018.

[7] D. Yang and S. Nam, "Electronically beamscannable sinusoidally modulated reactance surface antenna," *EPJ Appl. Metamater.*, vol. 6, p. 13, Mar. 2019.

[8] X. Wan, T. Y. Chen, X. Q. Chen, L. Zhang, and T. J. Cui, "Beam forming of leaky waves at fixed frequency using binary programmable metasurface," *IEEE Trans. Antennas Propag.*, vol. 66, no. 9, pp. 4942–4947, Sep. 2018.

[9] Z. Li, Y. J. Guo, S.-L. Chen, and J. Wang, "A period-reconfigurable leaky-wave antenna with fixed-frequency and wide-angle beam scanning," *IEEE Trans. Antennas Propag.*, vol. 67, no. 6, pp. 3720–3732, Jun. 2019.

[10] O. Yurduseven, D. L. Marks, J. N. Gollub, and D. R. Smith, "Design and analysis of a reconfigurable holographic metasurface aperture for dynamic focusing in the Fresnel zone," *IEEE Access*, vol. 5, pp. 15055–15065, 2017.

[11] O. Yurduseven, D. L. Marks, T. Fromenteze, and D. R. Smith, "Dynamically reconfigurable holographic metasurface aperture for a mills-cross monochromatic microwave camera," *Opt. Exp.*, vol. 26, no. 5, pp. 5281–5291, 2018.

[12] R.-B. Hwang, "Binary meta-hologram for a reconfigurable holographic metamaterial antenna," *Sci. Rep.*, vol. 10, no. 1, pp. 1–10, May 2020.

[13] M. Boyarsky, M. Imani, and D. Smith, "Grating lobe suppression in metasurface antenna arrays with a waveguide feed layer," *Opt. Exp.*, vol. 28, no. 16, pp. 23991–24004, Aug. 2020.

[14] M. Boyarsky, T. Sleasman, M. F. Imani, J. N. Gollub, and D. R. Smith, "Electronically steered metasurface antenna," *Sci. Rep.*, vol. 11, no. 1, pp. 1–10, Feb. 2021.

[15] B.-J. Che, F.-Y. Meng, Y.-L. Lyu, Y.-Q. Zhao, and Q. Wu, "Reconfigurable holographic antenna with low sidelobe level based on liquid crystals," *J. Phys. D, Appl. Phys.*, vol. 53, no. 31, Jul. 2020, Art. no. 315302.

[16] M. C. Johnson, S. L. Brunton, N. B. Kundtz, and J. N. Kutz, "Sidelobe canceling for reconfigurable holographic metamaterial antenna," *IEEE Trans. Antennas Propag.*, vol. 63, no. 4, pp. 1881–1886, Apr. 2015.

[17] A. Oliner and A. Hessel, "Guided waves on sinusoidally-modulated reactance surfaces," *IRE Trans. Antennas Propag.*, vol. 7, no. 5, pp. 201–208, Dec. 1959.

[18] B. H. Fong, J. S. Colburn, J. J. Ottusch, J. L. Visher, and D. F. Sievenpiper, "Scalar and tensor holographic artificial impedance surfaces," *IEEE Trans. Antennas Propag.*, vol. 58, no. 10, pp. 3212–3221, Oct. 2010.

[19] G. Minatti, F. Caminita, E. Martini, M. Sabbadini, and S. Maci, "Synthesis of modulated-metasurface antennas with amplitude, phase, and polarization control," *IEEE Trans. Antennas Propag.*, vol. 64, no. 9, pp. 3907–3919, Sep. 2016.

[20] A. M. Patel and A. Grbic, "A printed leaky-wave antenna based on a sinusoidally-modulated reactance surface," *IEEE Trans. Antennas Propag.*, vol. 59, no. 6, pp. 2087–2096, Jun. 2011.

[21] B. B. Tierney and A. Grbic, "Arbitrary beam shaping using 1-D impedance surfaces supporting leaky waves," *IEEE Trans. Antennas Propag.*, vol. 63, no. 6, pp. 2439–2448, Jun. 2015.

[22] D. R. Smith, O. Yurduseven, L. P. Mancera, P. Bowen, and N. B. Kundtz, "Analysis of a waveguide-fed metasurface antenna," *Phys. Rev. A, Gen. Phys.*, vol. 8, no. 5, Nov. 2017, Art. no. 054048.

[23] L. Pulido-Mancera, P. T. Bowen, M. F. Imani, N. Kundtz, and D. Smith, "Polarizability extraction of complementary metamaterial elements in waveguides for aperture modeling," *Phys. Rev. B, Condens. Matter*, vol. 96, no. 23, Dec. 2017, Art. no. 235402.

[24] R. Jakoby, A. Gaebler, and C. Weickhmann, "Microwave liquid crystal enabling technology for electronically steerable antennas in SATCOM and 5G millimeter-wave systems," *Crystals*, vol. 10, no. 6, p. 514, Jun. 2020.

Hyungcheol Kim received the B.S. degree in electrical and computer engineering from Seoul National University, Seoul, South Korea, in 2018, where he is currently pursuing the integrated master's and Ph.D. degrees with the Department of Electrical and Computer Engineering.

His current research interests include metamaterial-based antennas and reconfigurable beam-steering antennas.

Sangwook Nam (Senior Member, IEEE) received the B.S. degree in electrical engineering from Seoul National University, Seoul, South Korea, in 1981, the M.S. degree in electrical engineering from the Korea Advanced Institute of Science and Technology (KAIST), Seoul, in 1983, and the Ph.D. degree in electrical engineering from The University of Texas at Austin, Austin, TX, USA, in 1989.

From 1983 to 1986, he was a Researcher with the Gold Star Central Research Laboratory, Seoul. Since 1990, he has been a Professor with the School of Electrical Engineering and Computer Science, Seoul National University. His current research interests include the analysis/design of electromagnetic structures, antennas, and microwave active/passive circuits.